Open Access

This article is licensed under CC-BY 4.0 ⓒ ①

Article

On-Cell Saturation Transfer Difference NMR Spectroscopy on Ion Channels: Characterizing Negative Allosteric Modulator Binding Interactions of P2X7

Serena Monaco,* Jacob Browne, Matthew Wallace, Jesús Angulo,* and Leanne Stokes*

Cite This: *J. Am. Chem. Soc.* 2025, 147, 32400−32411

Read Online

ACCESS | 📊 Metrics & More | 📰 Article Recommendations | ⓢ Supporting Information

ABSTRACT: P2X7 receptors are important drug targets involved in pathologies ranging from psychiatric disorders to cancer. Being membrane embedded receptors, they are more challenging for structural characterization, and at present, we only have a small number of X-ray and cryo-EM structures for P2X7 bound to antagonists. We demonstrate that saturation transfer difference (STD) NMR on live mammalian cells (on-cell STD NMR) overexpressing P2X7 receptors allows further structural insight on the complexes of P2X7 with two potent negative allosteric modulators, namely, AZ10606120 and JNJ-47965567, via the determination of the binding epitope mapping of the interactions,

e.g., the main region of contact between the ligand and the binding pocket. This approach, reported for the first time on membrane-embedded ion channels, in combination with molecular docking, allows us to propose the first NMR-validated ligand binding models for two antagonists as bound to human P2X7 receptors and to correlate the structural knowledge acquired with the pharmacology data. We highlight the transformative potential of this application to aid drug design efforts in a less resource-demanding fashion than X-ray crystallography and cryo-EM, and we envisage on-cell STD NMR to fast become an asset for structure−activity relationship studies helping knowledge-based development of efficient drugs targeting P2X7 and other ion channels/membrane-embedded proteins.
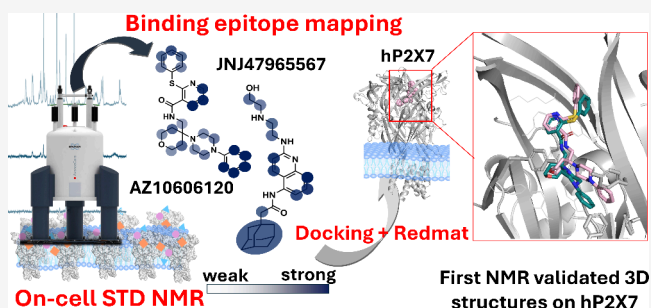
INTRODUCTION

P2X7 receptors are important ligand-gated ion channels highlighted as therapeutic targets for psychiatric disorders such as depression,[1] autism-spectrum disorders,[2,3] and cancer.[4] Ligand-gated ion channels respond to chemical molecules that interact with specific binding pockets on the channel complex. Once bound to the orthosteric site, agonist molecules induce conformational changes to the protein complex, allowing intrinsic ion channel pore opening. Allosteric sites also exist on ion channels, which can either hinder or enhance the ion channel opening mechanisms. X-ray crystallography has identified three identical intersubunit negative allosteric modulator (NAM) sites on P2X7 capable of accepting a diverse array of chemicals, as demonstrated by crystal structures of five antagonists in complex with giant panda P2X7,[5] cryo-EM structures of rat P2X7 bound to multiple antagonists,[6] and more recently, human P2X7 bound to a novel compound.[7] These sites are located behind the three orthosteric ATP sites, where the allosteric modulator can hinder ATP-driven conformational changes by acting as molecular wedges.[5]

Many antagonists have been developed for P2X7 by multiple pharmaceutical companies and academic groups.[8] Several P2X7 antagonists have progressed into clinical trials including

AZD9056[9,10] and CE-224,535[11] for rheumatoid arthritis and Crohn's disease, GSK1482160 (Phase I),[12] and JNJ-54175446 (current Phase II trials for depressive disorders)[13] although none have yet been taken further. Some pharmacological studies have used mutagenesis of the NAM binding site on hP2X7 to confirm the involvement of the NAM site in antagonist effects.[14,15] There is currently only one cryo-EM structure of human P2X7 in complex with an antagonist.[7] Furthermore, some antagonists display large species-dependent differences in activity while others display only subtle differences in potency.

In an effort to advance the structural knowledge on human P2X7 and overcome the limitations of X-ray and cryo-EM to study membrane embedded receptors, we have used saturation transfer difference (STD) NMR spectroscopy to study NAM antagonists binding to interspecies P2X7 receptors in solution.[16] To the best of our knowledge, this is the first
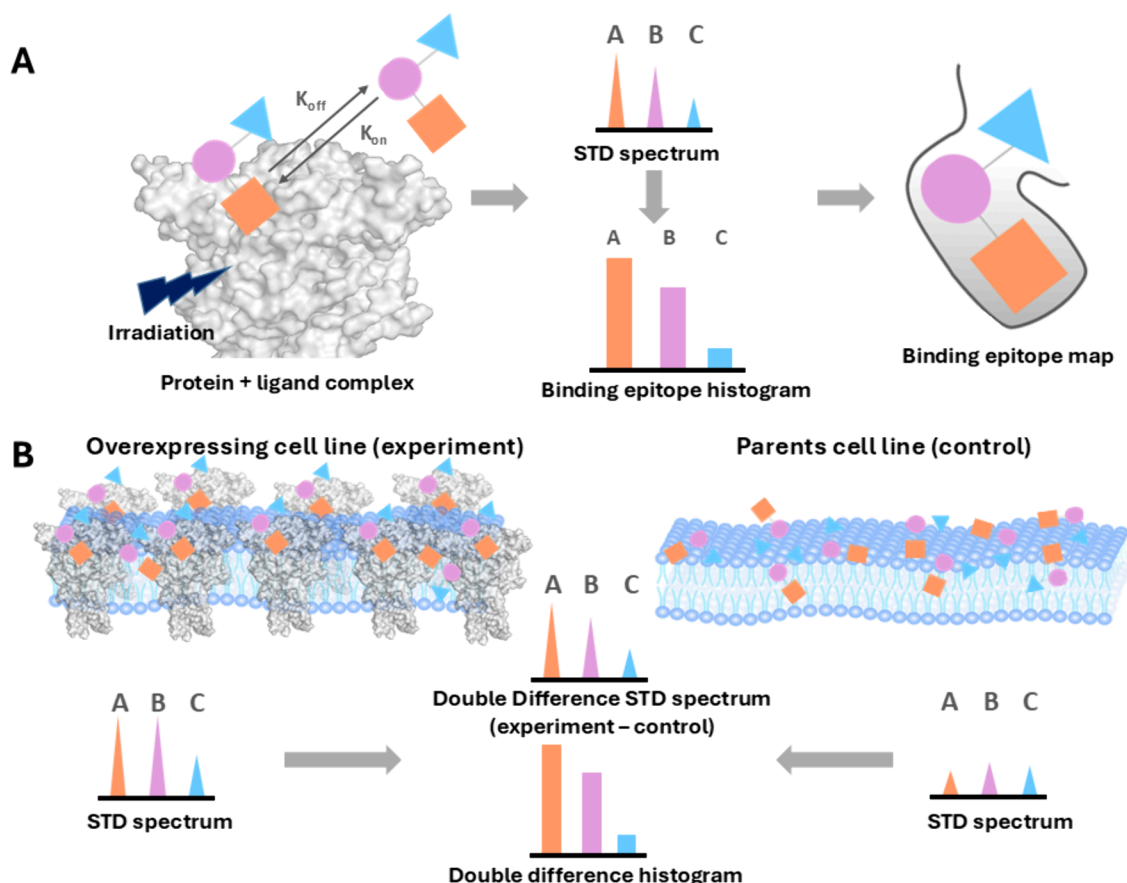
Figure 1. Principles behind on-cell STD NMR. (A) Representation of binding epitope map determination by STD NMR. (B) Representation of double-difference STD NMR, a necessary variation of the technique for on-cell STD NMR experiments, to eliminate signals resulting from the ligand interacting with the cell membrane.

example of the use of STD NMR to study membrane-embedded ion channels in living cells. Traditionally, STD NMR[17] has been used to study protein−ligand interactions in solution. It relies on the selective saturation of the protein, which is then transferred to the ligand, causing a reduction in the ligand NMR signal intensities. The STD NMR spectra are obtained as the difference of the reference NMR spectra (where selective saturation is off-resonance) minus the on-resonance-irradiated NMR spectra. Importantly, the STD intensity for each ligand proton is quantitatively related to the proximity of the given ligand proton to the protein surface. This allows one to determine the so-called binding epitope, i.e., a map depicting the ligand protons in closer contact to the protein, informing on the ligand binding mode in the protein binding pocket (Figure 1).[18] This ligand-based NMR technique has been previously proposed to investigate ligand binding to an overexpressed receptor on the surface of live cells (rather than purified in solution).[19] In this way, the determination of ligand−protein interactions/contacts with the protein attached to the cell membrane or embedded within it is achieved without the need for sample manipulations, labels, or protein purification. This confers strong potential to the approach, as it can provide structural information about the biomolecular interactions in conditions close to their native-like environment.

To ensure cancellation of signals from residual ligand interactions with cell membranes or other proteins on the cell surface, it is necessary to carry out a double-difference (STDD

NMR) version of the experiment, carrying out the subtraction between the STD spectra obtained in the presence of the "positive" cell line overexpressing the receptor of interest and the STD spectra obtained with the "parent" cell line or control experiment.[19] This isolates, for each set of protons, the actual STD response coming from the specific interaction of the small molecule with the overexpressed receptor. Following pioneering work from Jimenez-Barbero and co-workers on DC-SIGN interactions,[20] several applications have exploited this approach, extending the technique from sole binding screening to on-cell STD binding epitope mapping.[21−23] A large part of these studies has focused on protein−glycan interactions, given the many crucial processes involving cell−pathogen, cell−cell, and cell−matrix interactions, mostly taking place through surface proteins.

In this work, we have applied on-cell STD NMR to determine small molecule ligand binding epitope mapping for the *membrane-embedded* P2X7 ion channel overexpressed in HEK-293 cells. We have characterized the interactions of P2X7 with two well studied NAMs, AZ10606120 and JNJ-47965567, for which crystal structures are available for the related giant panda P2X7 (pdb entries: 5u1w, 5u1x)[5] and a cryo-EM structure, for JNJ-47965567 at rat P2X7 (pdb entry: 8TRB).[6] To understand the effect on the ligand−protein interactions upon mutation of the NAM site, we analyzed P2X7 from different species (human, mouse, and rat) as well as human P2X7 carrying mutations in the NAM pocket by generating clonal cell lines expressing three signature P2X7 NAM-site

mutations (F88A, M105A and F103A).[5,14] For the first time in an on-cell STD NMR study, we have used computational docking to propose 3D molecular models of the antagonists AZ10606120 and JNJ-47965567 binding at human, rat, and mouse P2X7 homology models and we validated these against the on-cell STD NMR data using a recently disclosed reduced relaxation matrix approach (RedMat) that allows time-efficient prediction of STD binding epitope mappings from 3D molecular models.[24]

Our approach provides structural insights on the human and rodent P2X7 receptors in complex with P2X7 antagonists. We also demonstrate that binding orientations determined by STD NMR can be correlated with pharmacological data and, thus, understand how differences in potency arise between different allosteric modulators across species and mutants.

■ METHODS

Cell Culture. Genetically edited HEK-293 cells lacking P2Y2 receptors were used to generate stable cell lines expressing human P2X7 (hP2X7), mouse P2X7 (mP2X7), rat P2X7 (rP2X7), or mutants of the hP2X7 NAM site (F88A, M105A, and F103A). Transfection was performed using lipofectamine 2000 (Fisher Scientific), and cells were subjected to Geneticin (800 μg/mL) selection for 2−3 weeks. This was followed by single cell cloning by limiting dilution in 96-well plates. Individual clones were selected for further study based on ATP-induced TO-PRO-3 uptake on a BD Cytoflex flow cytometer. Cell lines were maintained in DMEM:F12 media supplemented with 10% fetal bovine serum (PanBiotech), penicillin and streptomycin (Fisher Scientific) and kept in a humidified incubator with 5% CO_2. Stable P2X7-expressing cells were kept under Geneticin selection at a concentration of 400 μg/mL. Passaging was performed twice weekly using 0.25% Trypsin-EDTA (Fisher Scientific).

Intracellular Calcium Measurements. P2X7 responses were measured by monitoring intracellular calcium responses using fura-2AM loaded cells. Cells were plated at $2−2.5 \times 10^4$ cells/well the day before experiments in 96-well plates (NUNC) coated with 50 μg/mL poly-D-lysine (Merck Millipore). A loading buffer containing 2 μM fura-2AM (HelloBio) and 250 μM sulfinpyrazone (Merck Millipore) in a low divalent buffer (145 mM NaCl, 5 mM KCl, 0.2 mM $CaCl_2$, 10 mM HEPES, 13 mM glucose, pH 7.3) was added to cells for 45 min at 37 °C. After loading, the buffer was removed and replaced with calcium-containing extracellular solution (145 mM NaCl, 5 mM KCl, 2 mM $CaCl_2$, 10 mM HEPES, 13 mM glucose, pH 7.3). Responses were measured using a Flexstation 3 plate reader (Molecular Devices) with dual excitation wavelengths of 340 and 380 nm and single emission wavelength of 510 nm. The sample interval was 3.5 s, and each well was recorded for 180 s. Fura-2 ratios were calculated in Softmax Pro v5.4; zero baseline was applied, and responses were measured as normalized area under the curve (AUC). Dose inhibition curves were plotted using GraphPad Prism v6 nonlinear regression (three parameter fit) and log IC_{50} values reported.

Cell Preparation for STD NMR. Cells were grown to confluency in 10 cm tissue culture Petri dishes (Greiner) in DMEM:F12 complete media containing 400 μg/mL Geneticin. 0.25% trypsin-EDTA was used to dissociate cells, and fresh media was used to inactivate trypsin. Cells were then washed twice in PBS using centrifugation at 350g and washed in deuterated-PBS (1 mL). Cells were resuspended in 450 μL of deuterated-PBS and carefully counted using a hemocytometer. For each NMR experiment, 2 million cells in a total volume of 450 μL was used, and ligand was added to 0.3 mM concentration. For JNJ-47965567, DMSO-d_6 was added to aid solubility (40 μL), and the volume of deuterated-PBS was adjusted accordingly.

Antagonist NMR Assignment and STD NMR Analysis. All the NMR experiments were recorded at ^{1}H frequency of 800.23 MHz with a Bruker Avance III spectrometer equipped with a 5 mm probe TXI 800 MHz H-C/N-D-05 Z BTO. First, the antagonists

AZ10606120 and JNJ-47965567 were analyzed by 1D and 2D NMR in their free state and assigned using standard [1]H−^{1}H COSY (*cosydfesgpph*) and [1]H−^{13}C HSQC (*hsqctgpsp*) experiments at 293 K.

For STD NMR experiments, the samples were prepared as described in the above section; the temperature was set at 293 K, and the NMR tubes were kept spinning in the probe for the entire duration of the experiment to ensure that the cells stayed in suspension. An STD pulse sequence that included 2.5 and 5 ms trim pulses and a 3 ms spoil gradient and water suppression by excitation sculpting with gradients was used (*stddiffesgp.3*). Saturation was achieved by applying a train of 50 ms Gaussian pulses (0.40 mW) on the f2 channel at 0 ppm (on-resonance experiments) and 40 ppm (off-resonance experiments). The broad protein signals were removed by using a 40 ms spinlock ($T_{1\rho}$) filter. The experiments were performed at the single saturation time of 2 s with a d1 delay of 3 s, with 4 dummy scans and 192 scans, to keep the total duration of the experiment to 35 min. Control experiments with a 6 s d1 delay were performed to make sure that the d1 did not affect the binding epitope. STD NMR experiments were performed in duplicate for each ligand in the presence of each positive and negative parent cell line. Biological replicates were performed from distinct cell culture plates on different days.

Binding epitopes were obtained by determining the STD% for each ligand signal (corresponding to one or more protons depending on signal overlapping). The analysis was performed for the "positive" cell lines and the parent "negative" cell line separately, and the double difference was performed on the processed STD% for each biological duplicate. The double differences were then averaged between the duplicates and normalized to the most intense one for each complex (for which 100% is arbitrarily assigned). Error bars on the normalized STD percentage bar charts have been calculated by determining the standard deviation of the raw STD values for each atom (before normalization) and then normalizing each standard deviation to the percentage STD value.

Computational Docking and Analysis. Homology models for human P2X7 and mouse P2X7 were prepared using the SWISS model and template structure 5u1l. The cryo-EM structure of rat P2X7 (PDB 6u9v) was truncated at amino acid residue 401 and minimized in Maestro using the OPLS4 force field. Similar relaxation was performed for the hP2X7 and mP2X7 models. Template-based docking was performed using CBdock2 (https://cadd.labshare.cn/cb-dock2/index.php), a web-accessible version of Autodock Vina, for AZ10606120 and JNJ-47965567 aligning with database templates such as pdb 5u1l. Only one docking pose was generated using this approach.

RedMat. Docking poses were reviewed using RedMat (http://redmat.iiq.us-csic.es/), which uses a reduced relaxation matrix approach to predict binding epitope mappings of ligands in complex with a receptor protein. Docking poses were first processed by removing atom charges and renumbering ligand atoms so as to prevent any numerical overlap with the receptor protons. A complex correlation time of 50 ns was used together with a ligand concentration of 0.3 mM, a receptor concentration of 50 μM, a complex dissociation constant of 0.01 μM, and a cutoff distance of 12 Å. Methyl protons were selected to be selectively irradiated, and the spectrometer ^{1}H frequency used was 800 MHz. R-NOE factors were calculated following the equation for each set of experimental and predicted data.

$$\text{R-NOE} = \sqrt{\frac{\sum (\text{STD\%}_{\text{exp}} - \text{STD\%}_{\text{calc}})^2}{\sum (\text{STD\%}_{\text{exp}})^2}}$$

■ RESULTS

To perform the on-cell STD NMR experiments, we used HEK-293 cells overexpressing hP2X7 as the "positive" cell line and nonexpressing HEK-293 cells as the "negative" cell line (control background) for subtraction. We established a protocol involving several washes to remove traces of media
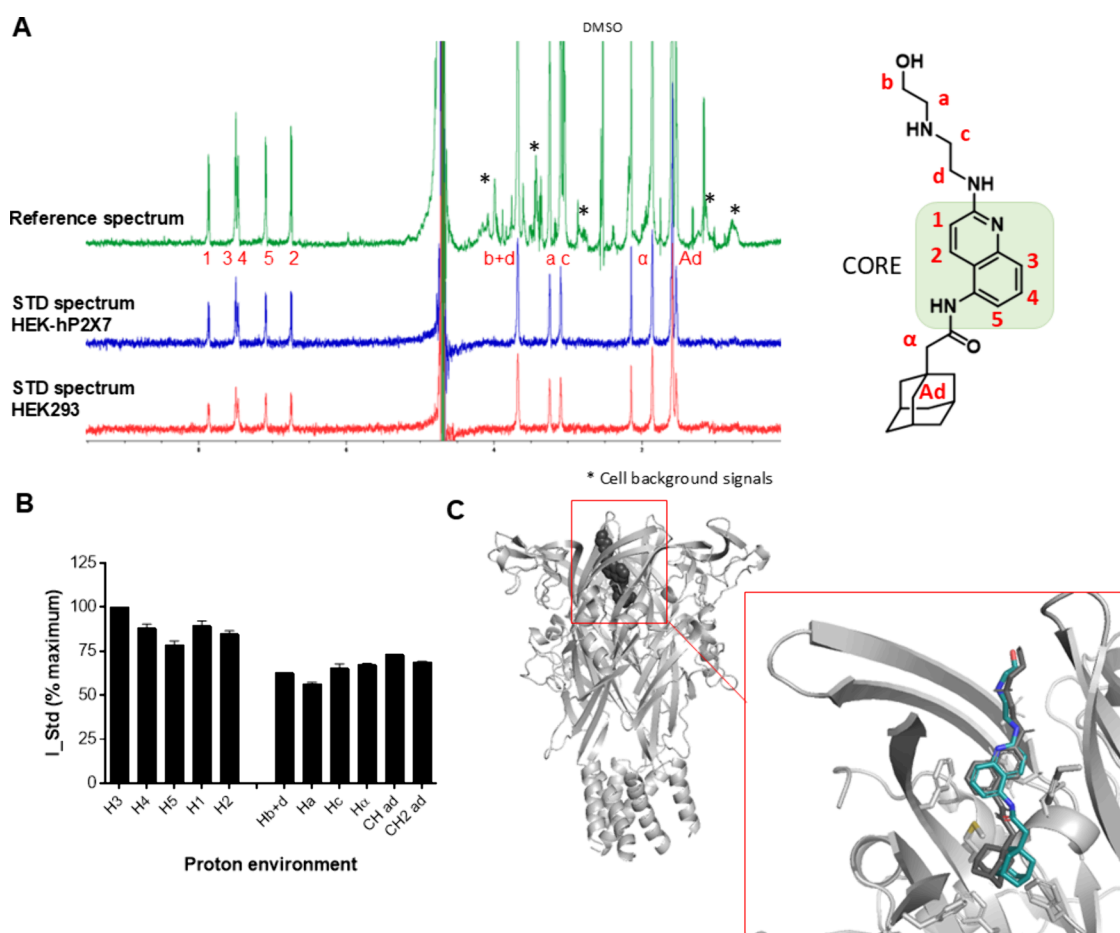
Figure 2. Binding profile of AZ10606120 and human P2X7 in living cells by STD NMR. (A) Unprocessed STD NMR spectra for AZ10606120; proton assignment and atom naming for AZ10606120 are shown. * indicates background signals from cells, and DMSO peak is labeled. (B) Histogram reporting the normalized binding epitope for the interaction of AZ10606120 with human P2X7. Error bars represent standard deviation of 2 replicates. (C) Comparison of the docking pose for AZ10606120 to hP2X7 homology model (in gray) with the X-ray structure with pdP2X7 (in cyan) (pdb: 5u1w).[5]

and equilibrate cells into deuterated-PBS. A careful cell count was critical, and the number of cells in the positive and the negative cell line was kept equivalent with 2 million cells routinely used. Once the ligand was added at a concentration of 0.3 mM, the cells were placed into the spectrometer (800 MHz) and STD NMR experiments were performed at a single saturation time (2 s), as described in the Methods. Critically, each experiment lasted 35 min and was performed while spinning the NMR sample tube to ensure the cells were well suspended in the buffer.

On-Cell STD NMR and Docking Studies on WT hP2X7 in Complex with AZ10606120 and JNJ-47965567. In Figure 2A, the 1D NMR spectra for AZ10606120 are shown together with the assignment of protons (double difference spectra can be found in Supplementary Figure 1). STD% was extracted for each set of protons in the positive and negative samples, and then, their values were subtracted. The proton with the highest STD was arbitrarily assigned a 100% value in the epitope mapping process, and the remaining intensities were normalized relative to that. Figure 2B shows a histogram depicting the binding epitope of AZ10606120 (each bar corresponds to the normalized STD intensities of each given proton set with error bars displaying variability between replicates). Two ligand binding regions were clearly identified: a "core" region with strong saturation transfer (the quinoline

moiety) and two areas with weaker saturation transfer, i.e., the aliphatic tail ("a", "b", "c", and "d" in Figure 2B) and the adamantane moiety ("ad" in Figure 2B). We compared the ligand pose in the crystal structure of AZ10606120 at pdP2X7 (pdb: 5u1w)[5] and the result from the computational docking of AZ10606120 to a human P2X7 homology model (Figure 2C) and used RedMat[24] to correlate the experimental on-cell STD NMR binding epitope data to the predicted computational pose. RedMat simulates the ligand binding epitope mapping from a 3D molecular model of a protein–ligand complex and compares it with the experimental data. Then, the so-called R-NOE factor evaluates the agreement between the predicted and the experimentally determined epitope map. As a rule of thumb, R-NOE values close to 0.3 are typically considered to be indicative of good agreement[24] and hence supporting experimental validation of the proposed 3D model. Since we are dealing with cells, a much more complex system than a sample containing a purified protein and ligand, we made the R-NOE threshold more flexible and considered structures with R-NOE values up to 0.35 as validated and refute those structures for which R-NOE was >0.36. The R-NOE value for AZ10606120 as bound to hP2X7 was 0.22, suggesting excellent correlation with the experimental data.

We performed the same experiments for binding of JNJ-47965567 to hP2X7 and report the ligand binding epitope
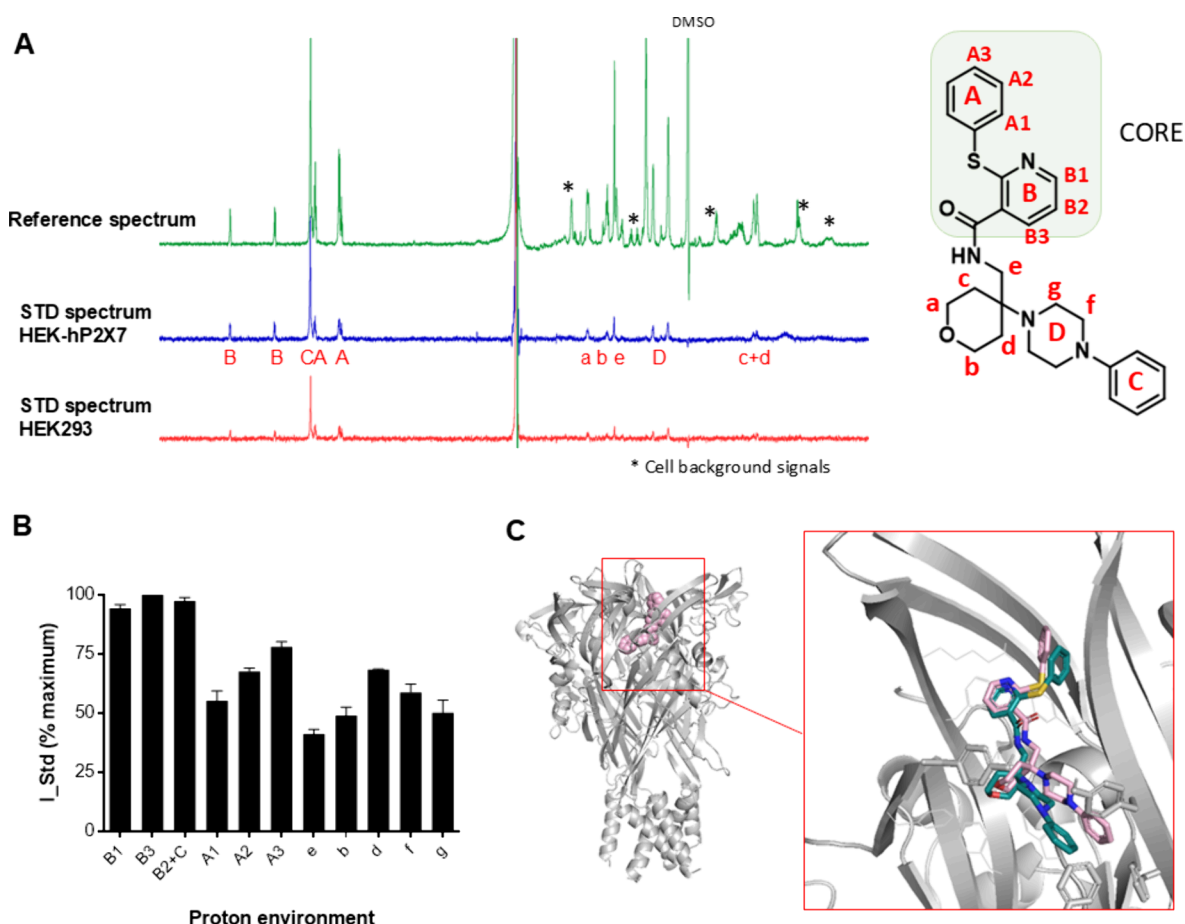
Figure 3. Binding profile of JNJ-47965567 and human P2X7 in living cells by STD NMR. (A) Unprocessed STD NMR spectra for JNJ-47965567, proton assignment, and atom nomenclature. * indicates background signals from cells, and the DMSO peak is labeled. (B) Histogram reporting the normalized binding epitope for JNJ-47965567. Error bars represent standard deviation of 2 replicates. (C) Comparison of the docking pose for JNJ-47965567 to hP2X7 (in pink) with the X-ray structure with pdP2X7 (in cyan) (pdb: 5u1x).[5]

derived from raw NMR data (Figure 3A,B) (double difference spectra can be found in Supplementary Figure 2). The STD NMR binding epitope analysis shows that the core region for JNJ-47965567 involves ring B and the sulfur linker to ring A. We also compared the crystal structure of JNJ-47965567 at pdP2X7 (pdb: 5u1x)[5] and the computational docking of JNJ-47965567 to a human P2X7 homology model (Figure 3C).

When superimposing the docking poses for the two antagonists AZ10606120 and JNJ-47965567 (extracted from the two pdP2X7 crystal structures; pdb: 5u1x, 5u1w[5]), their core regions overlap (Supplementary Figure 3). For JNJ-47965567, the C-ring is deepest in the pocket (Figure 2C) and picks up very high saturation transfer, suggesting close proximity to the protein surface. The tetrahydropyran ring overlaps with the space occupied by the adamantane ring in AZ10606120 and has a weaker saturation transfer. We used RedMat to correlate the experimental on-cell STD NMR data for JNJ-47965567 to the predicted computational pose and the calculated R-NOE value was 0.34, indicating a reasonable agreement.

Pharmacology, On-Cell STD NMR and Docking Studies on AZ10606120 and JNJ-47965567 Binding to P2X7 Across Species (Human, Mouse, Rat). Once we established the ligand binding epitopes for AZ10606120 and JNJ-47965567 for their interactions with human P2X7, we explored the species differences between human and rodent

P2X7 receptors. By measuring intracellular calcium responses, we confirmed that agonist ATP has a similar effect at all three (Figure 4A). AZ10606120 is more potent at hP2X7 and has the lowest potency at mP2X7, while rP2X7 is intermediate (Figure 4B). IC$_{50}$ values for both antagonists are reported in Table 1. We acquired ligand binding epitopes by STD NMR for AZ10606120 interacting with rP2X7 and mP2X7 (Figure 4C,D). Comparing these binding epitopes to the binding epitope at hP2X7, we observe very minor differences in the "core" aromatic region of AZ10606120. This region makes the strongest contact with the protein, and this feature is conserved across the orthologs. On the contrary, the epitopes of both rP2X7 and mP2X7 AZ10606120 show lower saturation transfer to the aliphatic tail ("Hc") and to the adamantane moiety ("CH ad") (Figure 4C,D). With the biggest potency difference seen between human and mouse P2X7, these results suggest that 3 ligand contact points are likely responsible ("Hα", "CH ad", and "Hc") for the pharmacological difference.

Computational docking of AZ10606120 into the mP2X7 homology model and rP2X7 structure (pdb: 6u9v) shows a similar binding pose to the pdP2X7 crystal structure (Figure 4E). Here again, in agreement with the binding epitopes, the orientation and position of the core aromatic region is conserved, while the adamantane and tail moieties have slight shifts from the human and panda P2X7. Using RedMat to correlate the experimental on-cell STD NMR data to the
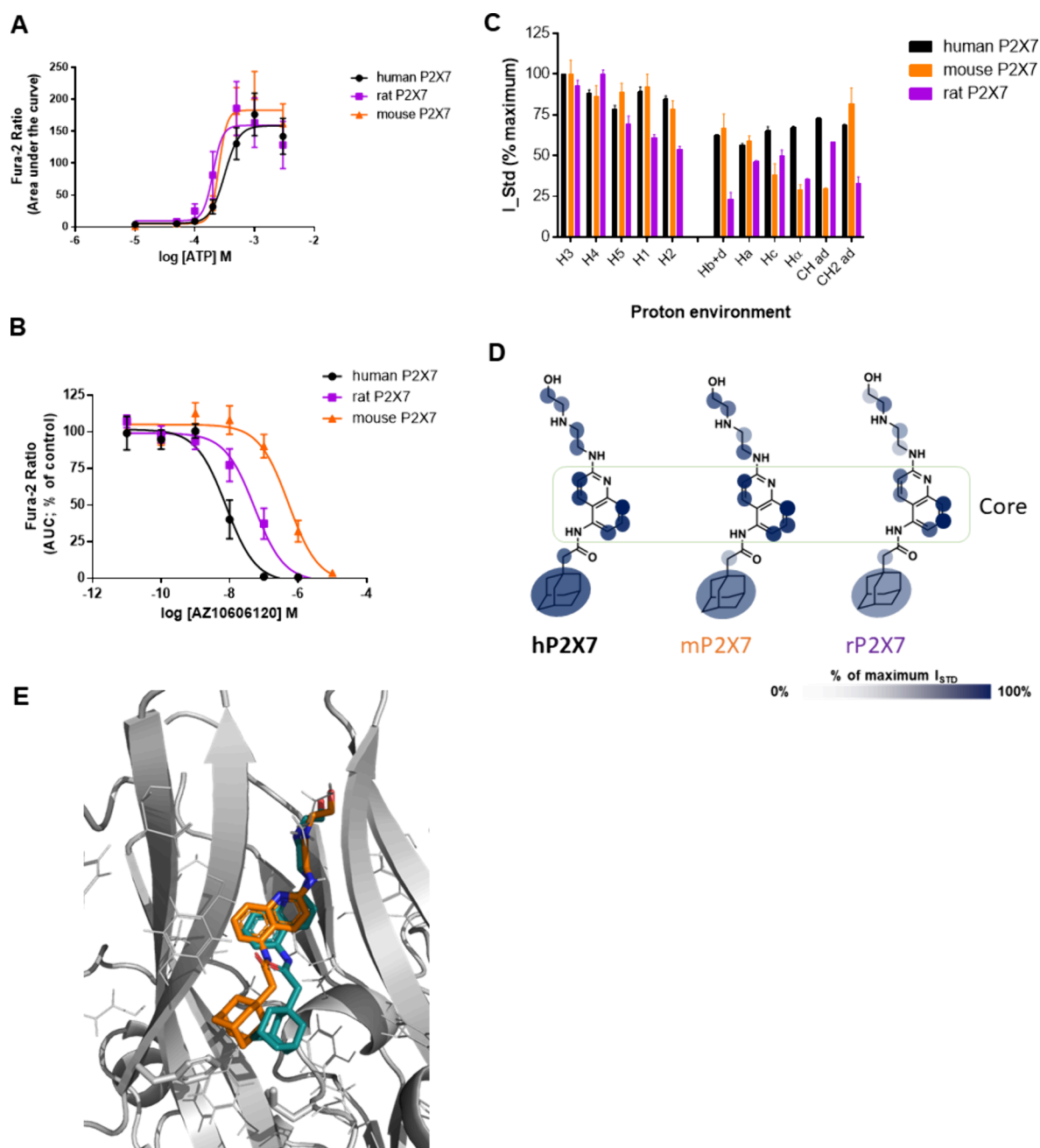
Figure 4. Pharmacology and binding profile of AZ10606120 interacting with rat and mouse P2X7 in living cells by STD NMR. (A) Concentration−response curve for ATP at P2X7 orthologs; human, rat, and mouse expressed in HEK-293 cells from a fura-2 calcium influx assay ($n = 3$ experiments). (B) Dose inhibition for AZ10606120 at P2X7 orthologs ($n = 3$ experiments). (C) Histogram reporting the normalized binding epitope for AZ10606120 at human (black), rat (purple), and mouse (orange) P2X7. Error bars represent standard deviation of 2 replicates. (D) Graphical representation of the binding epitope on the chemical structure of AZ10606120 using transparency to indicate strong and weak contact with the receptor. (E) Comparison of the template-based docking pose for AZ10606120 at mouse P2X7 (orange) with the X-ray structure of pdP2X7 (in cyan) (pdb: 5u1w).[5]

Table 1. Log IC$_{50}$ Values for P2X7 Antagonists Derived from the fura-2 Assay on Stable Cell Lines[a]

	AZ10606120 (nM)	JNJ-47965567 (nM)
Human P2X7	−8.10 ± 0.14 (7.9 nM)	−8.04 ± 0.10 (9.0 nM)
Rat P2X7	−7.28 ± 0.14 (53.1 nM)	−7.76 ± 0.08 (17.6 nM)
Mouse P2X7	−6.28 ± 0.15 (523.6 nM)	−6.90 ± 0.12 (125.4 nM)

[a]Standard error is indicated, and mean IC$_{50}$ is shown in brackets. From $n = 3$ independent experiments.

predicted computational poses, we achieved R-NOE values for AZ10606120 of 0.34 (mouse) and 0.54 (rat). This latter value

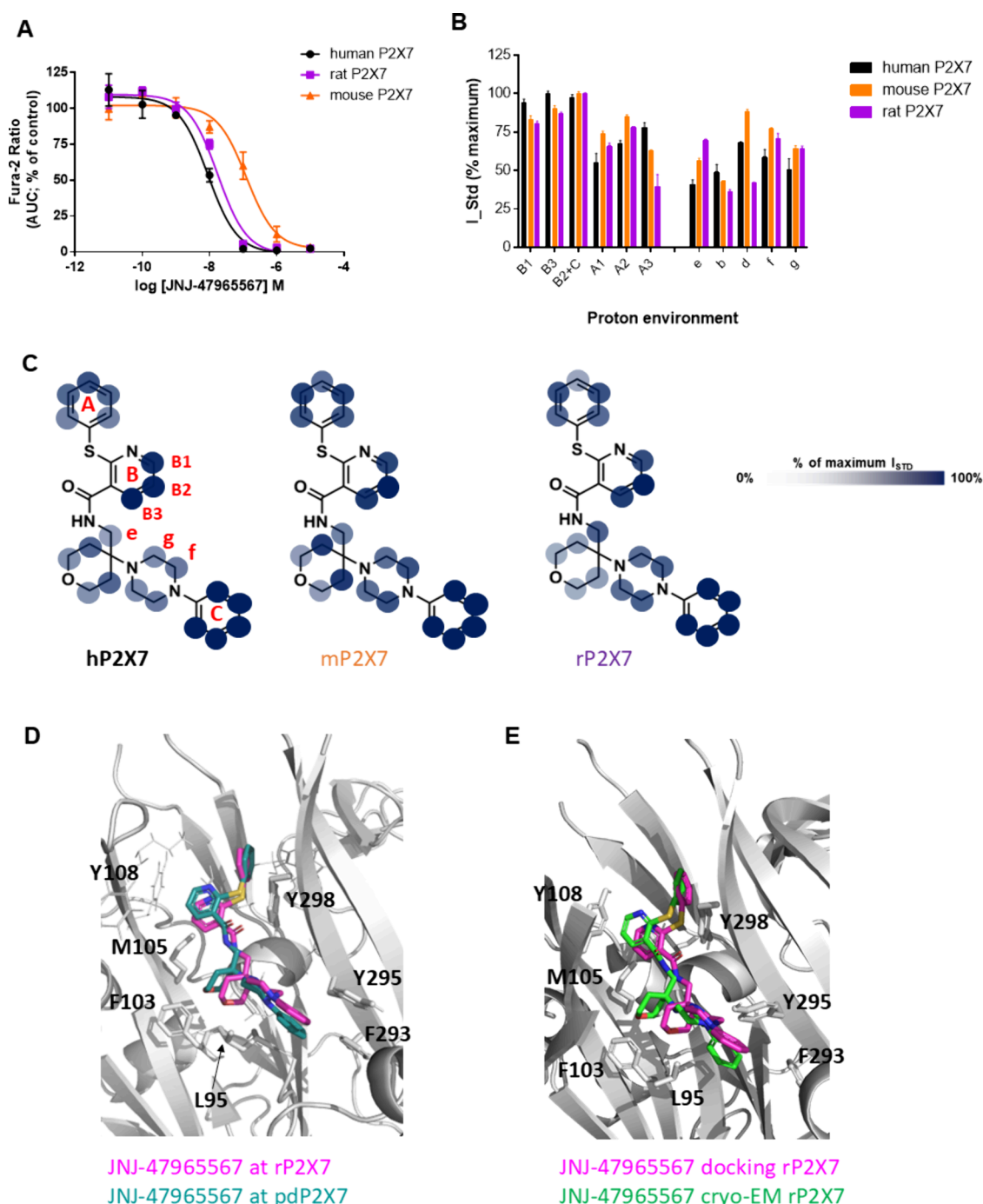indicates that the computational model cannot be validated with the experimental NMR data; hence, the structure is not

Figure 5. Pharmacology and binding profile of JNJ-47965567 interacting with rat and mouse P2X7 in living cells by STD NMR. (A) Dose inhibition for JNJ-47965567 at P2X7 orthologs (n = 3 experiments). (B) Histogram reporting the normalized binding epitope for JNJ-47965567 at human (black), rat (purple), and mouse (orange) P2X7. Error bars represent standard deviation of 2 replicates. (C) Graphical representation of the binding epitope on the chemical structure of JNJ-47965567 using transparency to indicate strong and weak contact with the receptor. (D) Comparison of the docking pose for JNJ-47965567 rat (magenta) with the X-ray structure with pdP2X7 (in cyan) (pdb: 5u1x).[5] (E) Comparison of the docking pose for JNJ-47965567 rat (magenta) with the cryo-EM structure of rP2X7 (in green) (pdb: 8TRB).[6] Key residues with side chains displayed are numbered.

included in Figure 4E. This suggests there are differences in how AZ10606120 engages with the NAM pocket in rP2X7.

We then performed the same analysis for the second antagonist: from intracellular calcium measurements, we determined that JNJ-47965567 had the highest potency at human P2X7 with the same rank order of potency as AZ10606120 (human > rat > mouse) (Figure 5A and Table 1), although the difference in IC$_{50}$ values was much smaller

here than for AZ10606120. Again, we performed computational docking of JNJ-47965567 into the mP2X7 homology model and rP2X7 structure (pdb: 6u9v).[25] The predicted binding orientation and position of JNJ-47965567 are similar with differences seen in rotation of ring A and placement of ring C (Figure 5D). From the on-cell STD NMR data, we can detect subtle changes in the ligand interactivity profile (Figure 5B), which must underlie the differences in pharmacological
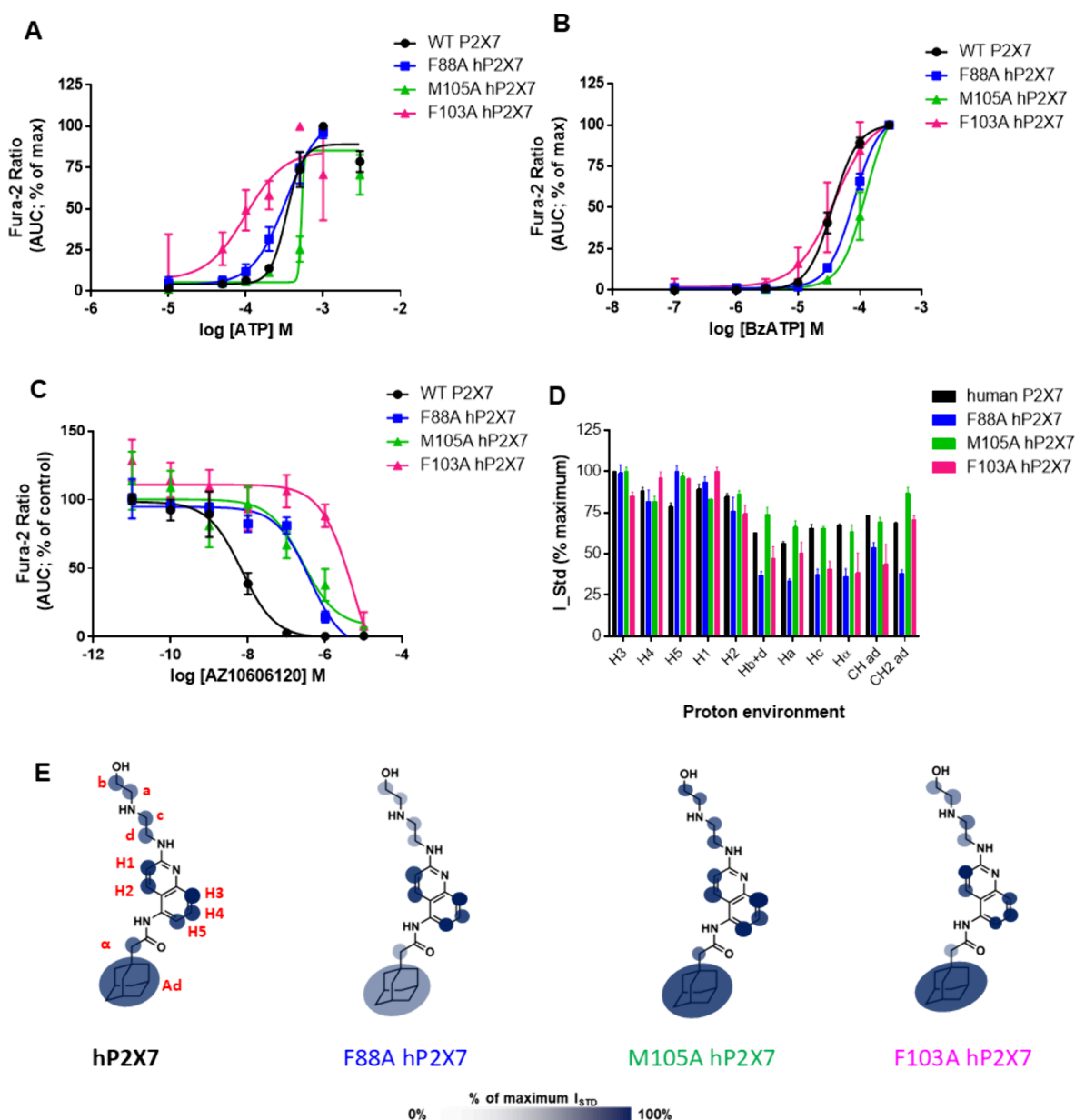
Figure 6. Pharmacology and binding profile of AZ10606120 interacting with WT hP2X7 and with P2X7 mutants M105A, F88A, and F103A. (A) Concentration−response curves to ATP and (B) concentration−response curves for BzATP for the mutant hP2X7 (n = 3 experiments). (C) Dose inhibition curve for AZ10606120 (n = 3 experiments). (D) Histogram reporting the normalized binding epitope for AZ10606120. Error bars represent standard deviation from 2 replicates. (E) Graphical representation of the binding epitope on the chemical structure of AZ10606120 using transparency to indicate strong and weak contact with the receptor.

effect. The proton assigned with maximal saturation (100%) is changed from "B3" (human) to "B2+C" (rat/mouse). For both "B1" and "B3", we observed lower saturation transfer suggestive of an altered engagement between the core and the protein surface. Increases in saturation transfer to "e", "f", and "g" agree with the predicted change in placement of rings C and D (Figure 5). Using RedMat to correlate the experimental on-cell STD NMR data to the predicted computational poses, we achieved R-NOE values for JNJ-47965567 of 0.36 (mouse) and 0.29 (rat). The recent cryo-EM model of JNJ-47965567 complexed with rat P2X7 (pdb 8TRB)[6] serves as a positive control for this work. Here, the resulting R-NOE value was 0.31, suggesting a good agreement between the cryo-EM structure and the experimental data. Indeed, these R-NOE values for docked JNJ-47965567 and the

cryo-EM structures are very similar and highlight the validity of on-cell STD NMR in reporting ligand binding profiles. Figure 5 shows comparisons between the docked pose for JNJ-47965567 and the reported cryo-EM structure.

Pharmacology, On-Cell STD NMR and Docking Studies on AZ10606120 and JNJ-47965567 Binding to P2X7 Across NAM-Site Mutants. After determining the ligand binding epitopes for AZ10606120 and JNJ-47965567 across orthologs, we explored differences across hP2X7 and selected NAM-site mutants. We chose to study three signature mutants M105A, F88A, and F103A, as they have been reported to affect potency of multiple NAMs.[5,14] Recently, it has been demonstrated that perturbations in ligand binding epitope mappings induced by strategic single point mutations in the binding site can be used to confirm binding location and gain

Table 2. Log IC$_{50}$ Values for P2X7 Antagonists at NAM-Site Mutants Derived from the fura-2 Assay with Standard Error[a]

| | AZ10606120 (nM) | | JNJ-47965567 (nM) | |
	ATP	BzATP	ATP	BzATP
WT hP2X7	−8.16 ± 0.14 (6.8 nM)	−7.65 ± 0.13 (22.5 nM)	−7.926 ± 0.08 (11.7 nM)	−7.59 ± 0.13 (26.0 nM)
F88A hP2X7	−6.41 ± 0.16 (392 nM)	−6.55 ± 0.16 (281 nM)	−6.917 ± 0.10 (125.3 nM)	−7.27 ± 0.20 (53.8 nM)
M105A hP2X7	−6.58 ± 0.34 (266 nM)	−6.20 ± 0.21 (636 nM)	−7.341 ± 0.28 (45.0 nM)	−7.54 ± 0.29 (28.7 nM)
F103A hP2X7	−5.21 ± 0.54 (6170 nM)	−5.44 ± 0.18 (3599 nM)	−6.81 ± 0.17 (161.1 nM)	−7.23 ± 0.10 (59.1 nM)

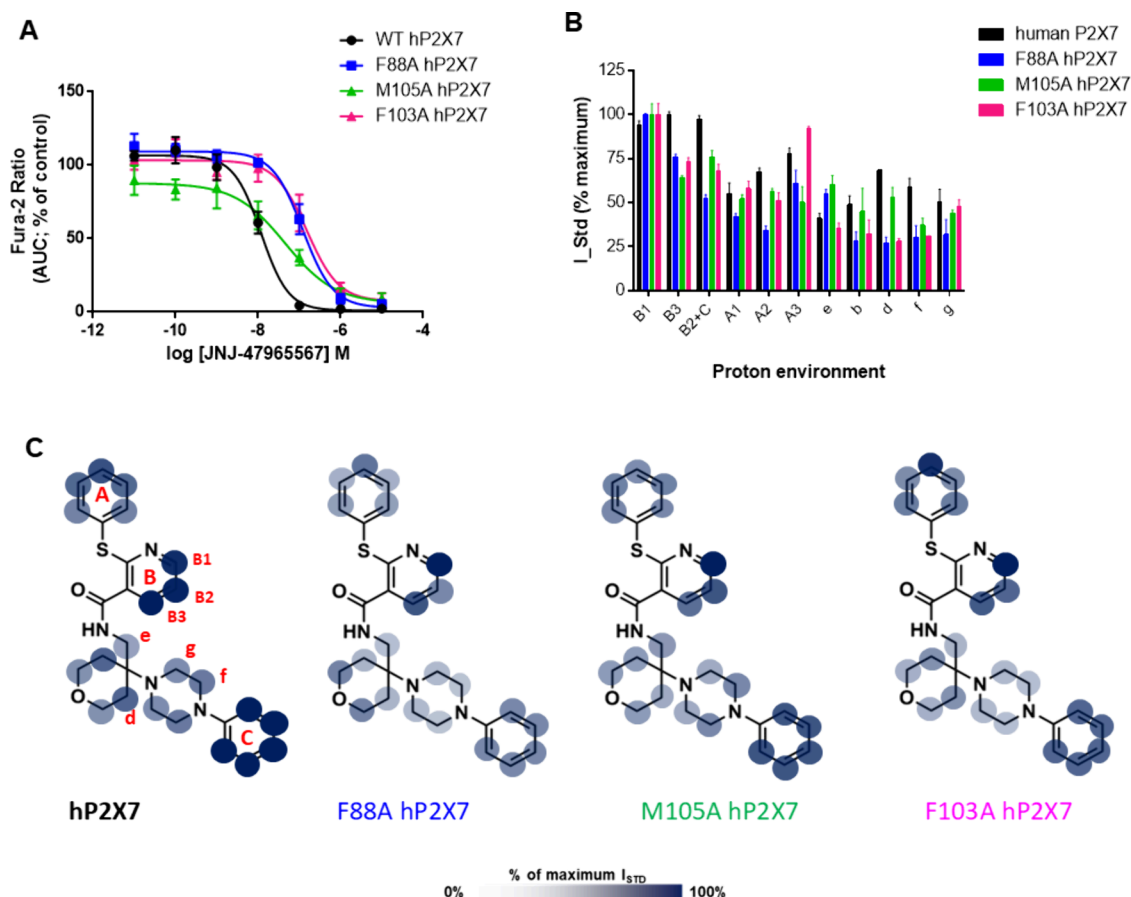[a]Mean IC$_{50}$ is in brackets. From $n = 3$ independent experiments.

Figure 7. Pharmacology and binding profile of JNJ-47965567 interacting with WT hP2X7 and with P2X7 mutants M105A, F88A, and F103A. (A) Dose inhibition curve for JNJ-47965567 ($n = 3$ experiments). (B) Histogram reporting the normalized binding epitope for JNJ-47965567. Error bars represent standard deviation of 2 replicates. (C) Graphical representation of the binding epitope on the chemical structure of JNJ-47965567 using transparency to indicate strong and weak contact with the receptor.

information on the ligand orientation in the binding pocket (Epitope-Perturbation-by-Mutation STD NMR).[26] We performed pharmacology studies with our overexpressed NAM-site mutant hP2X7 cell lines, including concentration response experiments to agonists ATP and BzATP to show that mutants were functional (Figure 6A,B). Dose inhibition curves show the effect on AZ10606120 potency as the NAM site is altered (Figure 6C) and IC$_{50}$ values are reported in Table 2. We confirmed a loss in potency for both antagonists with all three mutants. F88A and M105A show a similar loss in potency with IC$_{50}$ dropping to ~300 nM (from 6.8 nM), while F103A shows a major 1000-fold loss in potency. Figure 6D,E shows subtle changes in the AZ10606120 binding epitopes between hP2X7 and the NAM-site mutants. The proton assigned with maximal saturation (100%) is changed from "H3" (human wild-type) to "H5" (F88A) or "H1" (F103A) suggestive of an altered engagement between the core and the protein surface of the

mutant P2X7. Indeed, mutant F103A shows the most variation in saturation transfer to the core region compared to WT human P2X7 and has additional differences in both the aliphatic tail and adamantane moieties (Figure 6D), underpinning the large difference in pharmacological potency for this antagonist.

We performed computational docking for the mutants (see Supplementary Figure 4), and no dramatic variation from the binding mode at the wild-type hP2X7 was predicted using our template-based docking approach. RedMat analysis of these poses against the on-cell STD NMR data report R-NOE values of 0.29 (M105A), 0.38 (F88A), and 0.26 (F103A), validating the models of M105A- and F103A-hP2X7 ligand complexes.

Figure 7 shows the pharmacology and structural analysis for JNJ-47965567 with IC$_{50}$ values reported in Table 2. Similar to the species differences, we observed a much smaller loss in potency between hP2X7 and the NAM-site mutants for JNJ-

47965567 with only a 10-fold increase in IC$_{50}$ for F88A and F103A and a less than 5-fold increase for M105A-hP2X7. From the on-cell STD NMR data, we can detect changes in the ligand interactivity profile (Figure 5B) that must underlie the differences in pharmacological effect. The proton assigned with maximal saturation (100%) is changed from "B3" (human) to "B1" (mutants), and there is a considerable decrease in saturation transfer to "B3" and "B2+C", suggestive of an altered engagement between the core region and the protein surface. Reductions in saturation transfer to "d", "f", and "g" are also seen with F88A and F103A, which correlate with the biggest pharmacological difference seen.

The computational docking did not predict dramatic variations in the binding pose of JNJ-47965567 (Supplementary Figure 5), and from RedMat analysis, these poses do not correlate well with the on-cell STD NMR data. RedMat reports R-NOE values of 0.35 (M105A-hP2X7), 0.51 (F103A-hP2X7), and 0.57 (F88A-hP2X7), indicating that the computational predictions are likely to be inaccurate for F88A- and F103A-hP2X7.

DISCUSSION

Comparison of Binding Mode and Potency Across Species. With the publication of the crystal structure of pdP2X7 in complex with five different negative allosteric modulators,[5] a structural model of how such ligands engage with a mammalian P2X7 was first visualized. Overlaying these ligands can yield some information regarding key chemical groups, and looking at potential interactions can yield information about key interacting residues. Here, we provide for the first time experimental evidence that the overlapping "core" regions of AZ10606120 and JNJ-47965567 make the strongest contacts with the P2X7 protein membrane-embedded on living cells. The core regions are close to an aromatic-rich region of the NAM binding pocket composed of phenylalanine residues (88 and 108) and tyrosine 298. This suggests that aromatic−aromatic interactions could be the main factor for the high affinity interactions of these two ligands to the hP2X7 NAM binding pocket. JNJ-47965567 is more tightly bound into the NAM pocket with additional strong contacts being made with the deepest part of the molecule, the phenyl moiety on the piperazine ring (C-ring in Figure 3). Our on-cell STD NMR binding epitope mapping was corroborated by the docking poses obtained for the two ligands using an hP2X7 homology model and a template-based docking approach. The docking pose predicted is highly similar to the crystal structure of pdP2X7 in complex with AZ10606120 and JNJ-47965567 and is experimentally validated through calculation of a reduced relaxation matrix (RedMat) to predict the theoretical binding epitope maps from 3D molecular models of the protein−ligand complexes.[24]

Our investigations on P2X7 rodent homologues suggest that the central core of AZ10606120 makes interactions with the NAM pocket across species, whereas saturation transfer to the aliphatic tail and adamantane moiety of AZ10606120 is weaker for the rodent P2X7 receptors. A key difference between the mouse P2X7 and human P2X7 NAM-site is at amino acid 312, which is a valine in human but an alanine in mouse/rat. This substitution would cause the rodent NAM pocket to be slightly bigger, accounting for some loss of STD intensities for the adamantane moiety of AZ10606120 (Figure 4D). An additional difference between rat P2X7 and human P2X7 is amino acid 95, which is phenylalanine in human/mouse and leucine

in rat.[27] This residue sits at the very base of the NAM pocket and is also expected to interact with the adamantane moiety of AZ10606120. In the absence of F95, the rat NAM pocket would be bigger and provide a different electrostatic environment than the human and mouse P2X7 NAM-site, explaining the further loss of STD signal on the adamantane moiety. It is likely that, in the absence of the aromatic moiety of F95, the AZ10606120 ligand has a different orientation, but it cannot extend deeper into the pocket due to the core region interactions. Indeed, the docking poses confirm the hypothesis that the core region is "anchoring" the ligand at a fixed depth through aromatic−aromatic interactions in the lipophilic binding pocket, giving very little freedom for the ligand to rearrange and occupy the larger pockets in a more effective way. This can be mainly ascribed to the most rigid and linear character of AZ10606120, so that once it is "anchored", it cannot vary its orientation to occupy the space differently. This also implies that this ligand retains a similar position from the smaller human P2X7 NAM pocket to the larger rodent P2X7 NAM pocket. The higher R-NOE value (0.54) for the docking generated model of AZ10606120 at rP2X7 suggests that the docking pose for this complex is not representative of the binding mode of AZ10606120 in the much larger rat P2X7 NAM pocket. This is difficult to reconcile using computational docking, and further structural investigations (X-ray crystallography or cryo-EM) would be required to clarify this.

Looking closely at the biggest pharmacological difference for AZ10606120 (which is between human and mouse P2X7) to correlate this with the on-cell STD NMR data, we suggest that 3 major contact points of the ligand are responsible for this change in potency: "Hα", "CH ad", and "Hc". This information will be useful in a drug discovery program to improve the molecular fit to the rodent P2X7 NAM site, indicating that further chemical modifications should involve the aliphatic tail and adamantane moieties. We believe this highlights the validity of this approach in analyzing ligands during structure−activity relationship investigations.

For JNJ-47965567, the core region also receives high saturation transfer, a feature that is somewhat conserved across species, suggesting tight anchoring to the aromatic-rich region in the center of the P2X7 NAM binding pocket. We did observe that "B1" and "B3" showed lower saturation transfer, suggestive of an altered engagement between the core and the protein surface with increases in saturation transfer to "e", "f", and "g" protons also observed (Figure 5). The variability in pharmacological potency of JNJ-47965567 across species was less than that for AZ10606120 with only a 13-fold difference between hP2X7 and mP2X7 IC$_{50}$ values. However, we observed more variation in overall saturation transfer to JNJ-47965567 between hP2X7, mP2X7, and rP2X7, mostly seen at the tetrahydropyran−piperazine region. The tetrahydropyran ring of JNJ-47965567 overlaps with the adamantane moiety of AZ10606120 (Supplementary Figure 3), and in hP2X7, the adamantane moiety averages 70% STD intensity, whereas the tetrahydropyran ring has 50−70% STD intensities. Therefore, we see clear consistencies between the two ligands in the hP2X7 NAM pocket. With both the "core" and the deepest phenyl moiety of JNJ-47965567 being well anchored within the NAM pocket, this explains why there is little difference in pharmacological effect with this ligand (confirming that seen in ref 28) even though there is some variation in the architecture of NAM pocket across species. Certainly, the detailed ligand binding epitope provided by the on-cell STD NMR approach

is of great relevance to identify the regions available for chemical modification for a ligand to undergo further improvement.

Comparison of Binding Mode and Potency Across Mutants. Pharmacology and binding epitope analysis were performed for three hP2X7 mutants, namely, M105A, F88A, and F103A, for both AZ10606120 and JNJ-47965567 ligands. As expected from other studies,[14] we did observe a reduction in potency relative to the WT hP2X7 for the specific mutants selected, and this reduction was much more pronounced for AZ10606120 than for JNJ-47965567. As observed for the P2X7 orthologs, there was variation in binding epitopes for AZ10606120, some of which were again related to the aliphatic tail and adamantane moieties. We did observe altered saturation transfer to the core region of AZ10606120 with a switching of protons assigned with maximal saturation (100%) from "H3" (human) to "H5" (F88A) or "H1" (F103A). Focusing on F103A, these alterations in binding epitope are responsible for the large difference in pharmacological potency for this antagonist, and this technique is useful for highlighting how this mutation affects the antagonist interactivity with the P2X7 NAM-site surface.

With JNJ-47965567, there were similar alterations in the saturation transfer to the core region in mutants exhibiting the largest change in pharmacological potency (F88A, F103A). RedMat did not validate the poses at F88A-hP2X7 and F103A-hP2X7 against the STD NMR binding epitope data, suggesting that the crystal structure pdP2X7-like orientation of this ligand is not valid for these NAM-site mutants. In these cases, it may be that there are major alterations/rearrangements of the aromatic networks within the NAM pocket, which allows JNJ-47965567 to interact differently. This hypothesis is compatible with the reduction in the STD intensities associated with the deepest phenyl moiety (C-ring) for F88A-hP2X7 and F103A-hP2X7 plus changes in the core region.

CONCLUSION

Here, we show for the first time that saturation transfer difference (STD) NMR can be used on a mammalian cell line overexpressing a membrane-embedded ligand-gated ion channel to obtain ligand binding epitope mappings, gaining key structural insights on receptor–ligand interactions, in the native environment of the ion channel. We performed on-cell STD NMR for the structural investigation of antagonists as bound to P2X7 ion channels in their physiological membrane-bound environment. The use of the recently released RedMat software enabled us to combine the experimental binding epitope mappings obtained by on-cell STD NMR with molecular docking, proving this to be a ground-breaking approach in providing the first NMR-validated ligand binding models for AZ10606120 bound to hP2X7 and mP2X7 and JNJ-47965567 bound to hP2X7 and rP2X7. It is worth noticing the inexpensive and versatile nature of STD NMR (with an experiment duration of 35 min) relative to other structural techniques like X-ray crystallography and cryo-EM for membrane-embedded ion channels. While the capability of studying these biological systems in solution and in a native environment without the need for receptor purification and in higher throughput fashion are great advantages of this technique, it is important to highlight that this approach cannot substitute for the high-resolution detail and precision available with cryo-EM and X-ray crystallography and is suggested as a complementary technique. We have shown the

potential of on-cell STD NMR to pick up on differences in the binding mode upon binding pocket variation, and with some limitations, we have been able to correlate this to pharmacology data, paving the way for a wider applicability to structure–activity-relationship (SAR) studies for receptors embedded in live cells. This approach will be extremely useful for the design of new and successful drugs targeting ion channels and other embedded receptors, and we envisage this approach to become a new frontier in drug discovery.

■ ASSOCIATED CONTENT

Ⓢ Supporting Information

The Supporting Information is available free of charge at https://pubs.acs.org/doi/10.1021/jacs.5c02985.

Double difference STD NMR spectra for AZ10606120 and JNJ-47965567 with WT hP2X7 (Figures S1 and S2); comparison of AZ10606120 and JNJ-47965567 positions in the binding pocket from XRD of pdP2X7 (Figure S3); comparison of docking poses for AZ10606120 and JNJ-47965567 docked to WT or NAM-site mutant hP2X7 (Figures S4 and S5) (PDF)

■ AUTHOR INFORMATION

Corresponding Authors

Serena Monaco − *School of Chemistry, Pharmacy & Pharmacology, University of East Anglia, Norwich NR4 7TJ, United Kingdom; Quadram Institute, Norwich NR4 7UQ, United Kingdom;* ⓞ orcid.org/0000-0001-9396-7568; Email: Serena.Monaco@quadram.ac.uk

Jesús Angulo − *Instituto de Investigaciones Químicas (IIQ), Consejo Superior de Investigaciones Científicas and Universidad de Sevilla, Sevilla 41092, Spain;* ⓞ orcid.org/0000-0001-7250-5639; Email: j.angulo@iiq.csic.es

Leanne Stokes − *School of Chemistry, Pharmacy & Pharmacology, University of East Anglia, Norwich NR4 7TJ, United Kingdom;* ⓞ orcid.org/0000-0003-4013-6781; Email: l.stokes@uea.ac.uk

Authors

Jacob Browne − *School of Chemistry, Pharmacy & Pharmacology, University of East Anglia, Norwich NR4 7TJ, United Kingdom;* Present Address: Department of Pharmacology, University of Cambridge, Tennis Court Road, Cambridge, CB2 1PD

Matthew Wallace − *School of Chemistry, Pharmacy & Pharmacology, University of East Anglia, Norwich NR4 7TJ, United Kingdom;* ⓞ orcid.org/0000-0002-5751-1827

Complete contact information is available at:
https://pubs.acs.org/10.1021/jacs.5c02985

Notes

The authors declare no competing financial interest.

■ REFERENCES

(1) Deussing, J. M.; Arzt, E. P2X7 Receptor: A Potential Therapeutic Target for Depression? *Trends in Molecular Medicine* **2018**, *24* (9), 736−747.

(2) Horváth, G.; et al. P2X7 Receptors Drive Poly(I:C) Induced Autism-like Behavior in Mice. *J. Neurosci.* **2019**, *39* (13), 2542.

(3) Szabó, D.; et al. Maternal P2X7 receptor inhibition prevents autism-like phenotype in male mouse offspring through the NLRP3-IL-1β pathway. *Brain, Behavior, and Immunity* **2022**, *101*, 318−332.

(4) Lara, R. P2X7 in Cancer: From Molecular Mechanisms to Therapeutics. *Frontiers in Pharmacology* **2020**, *11*, 1.

(5) Karasawa, A.; Kawate, T. Structural basis for subtype-specific inhibition of the P2X7 receptor. *eLife* **2016**, *5*, No. e22153.

(6) Oken, A. C.; et al. P2X7 receptors exhibit at least three modes of allosteric antagonism. *Science Advances* **2024**, *10* (40), No. eado5084.

(7) Oken, A. C.; et al. UB-MBX-46 is a potent and selective antagonist of the human P2X7 receptor developed by structure-based drug design. *bioRxiv* **2025**, 2025.02.12.637899; DOI: 10.1101/2025.02.12.637899.

(8) Dane, C.; Stokes, L.; Jorgensen, W. T. P2X receptor antagonists and their potential as therapeutics: a patent review (2010−2021). *Expert Opinion on Therapeutic Patents* **2022**, *32* (7), 769−790.

(9) Eser, A.; et al. Safety and Efficacy of an Oral Inhibitor of the Purinergic Receptor P2X7 in Adult Patients with Moderately to Severely Active Crohn's Disease: A Randomized Placebo-controlled, Double-blind, Phase IIa Study. *Inflammatory Bowel Diseases* **2015**, *21* (10), 2247−2253.

(10) Keystone, E. C.; et al. Clinical evaluation of the efficacy of the P2X7 purinergic receptor antagonist AZD9056 on the signs and symptoms of rheumatoid arthritis in patients with active disease despite treatment with methotrexate or sulphasalazine. *Annals of the Rheumatic Diseases* **2012**, *71* (10), 1630.

(11) Stock, T. C.; et al. Efficacy and Safety of CE-224,535, an Antagonist of P2X7 Receptor, in Treatment of Patients with Rheumatoid Arthritis Inadequately Controlled by Methotrexate. *Journal of Rheumatology* **2012**, *39* (4), 720.

(12) Ali, Z.; et al. Pharmacokinetic and pharmacodynamic profiling of a P2X7 receptor allosteric modulator GSK1482160 in healthy human subjects. *Br. J. Clin. Pharmacol.* **2013**, *75* (1), 197−207.

(13) Recourt, K.; et al. Characterization of the central nervous system penetrant and selective purine P2X7 receptor antagonist JNJ-54175446 in patients with major depressive disorder. *Translational Psychiatry* **2023**, *13* (1), 266.

(14) Allsopp, R. C.; et al. Unique residues in the ATP gated human P2X7 receptor define a novel allosteric binding pocket for the selective antagonist AZ10606120. *Sci. Rep.* **2017**, *7* (1), 725.

(15) Bin Dayel, A.; Evans, R. J.; Schmid, R. Mapping the Site of Action of Human P2X7 Receptor Antagonists AZ11645373, Brilliant Blue G, KN-62, Calmidazolium, and ZINC58368839 to the Intersubunit Allosteric Pocket. *Mol. Pharmacol.* **2019**, *96* (3), 355.

(16) Mayer, M.; Meyer, B. Characterization of Ligand Binding by Saturation Transfer Difference NMR Spectroscopy. *Angew. Chem., Int. Ed.* **1999**, *38* (12), 1784−1788.

(17) Mayer, M.; Meyer, B. Group Epitope Mapping by Saturation Transfer Difference NMR To Identify Segments of a Ligand in Direct Contact with a Protein Receptor. *J. Am. Chem. Soc.* **2001**, *123* (25), 6108−6117.

(18) Angulo, J.; Nieto, P. M. STD-NMR: application to transient interactions between biomolecules—a quantitative approach. *Eur. Biophys. J.* **2011**, *40* (12), 1357−1369.

(19) Claasen, B.; et al. Direct Observation of Ligand Binding to Membrane Proteins in Living Cells by a Saturation Transfer Double Difference (STDD) NMR Spectroscopy Method Shows a Significantly Higher Affinity of Integrin αIIbβ3 in Native Platelets than in Liposomes. *J. Am. Chem. Soc.* **2005**, *127* (3), 916−919.

(20) Mari, S.; Jimenez-Barbero, J.; et al. 1D Saturation Transfer Difference NMR Experiments on Living Cells: The DC-SIGN/Oligomannose Interaction. *Angew. Chem., Int. Ed.* **2005**, *44* (2), 296−298.

(21) Palmioli, A.; et al. On-cell saturation transfer difference NMR for the identification of FimH ligands and inhibitors. *Bioorganic Chemistry* **2021**, *112*, No. 104876.

(22) Palmioli, A.; et al. Multivalent calix[4]arene-based mannosylated dendrons as new FimH ligands and inhibitors. *Bioorganic Chemistry* **2023**, *138*, No. 106613.

(23) Bertuzzi, S.; et al. Exploring Glycan-Lectin Interactions in Natural-Like Environments: A View Using NMR Experiments Inside Cell and on Cell Surface. *Chemistry − A European Journal* **2025**, *31* (10), No. e202403102.

(24) Nepravishta, R.; et al. Fast Quantitative Validation of 3D Models of Low-Affinity Protein−Ligand Complexes by STD NMR Spectroscopy. *J. Med. Chem.* **2024**, *67* (12), 10025−10034.

(25) McCarthy, A. E.; Yoshioka, C.; Mansoor, S. E. Full-Length P2X7 Structures Reveal How Palmitoylation Prevents Channel Desensitization. *Cell* **2019**, *179* (3), 659−670.E13.

(26) Ramírez-Cárdenas, J.; et al. STD NMR Epitope Perturbation by Mutation Unveils the Mechanism of YM155 as an Arginine-Glycosyltransferases Inhibitor Effective in Treating Enteropathogenic Diseases. *JACS Au* **2025**, *5* (3), 1279−1288.

(27) Michel, A. D.; et al. Identification of regions of the P2X7 receptor that contribute to human and rat species differences in antagonist effects. *Br. J. Pharmacol.* **2008**, *155* (5), 738−751.

(28) Bhattacharya, A.; et al. Pharmacological characterization of a novel centrally permeable P2X7 receptor antagonist: JNJ-47965567. *Br. J. Pharmacol.* **2013**, *170* (3), 624−640.